European Review for Medical and Pharmacological Sciences 2023; 27: 10749-10762

Specific role of NAD+ biosynthesis reduction mediated mitochondrial dysfunction in vascular endothelial injury induced by chronic intermittent hypoxia

Z.-T. FAN[1,3], L.-P. DONG[1], Y.-H. NIU[1], W.-W. CHI[1], G.-L. WU[2], D.-M. SONG[1,2]

[1]Clinical Biobank, The First Hospital of Hebei Medical University, Shijiazhuang, Hebei, China
[2]Department of Otolaryngology, The First Hospital of Hebei Medical University, Shijiazhuang, Hebei, China
[3]Department of Otolaryngology, Hebei Eye Hospital, Xingtai, Hebei, China

Abstract. – OBJECTIVE: Cardiovascular diseases (CVD) are prevalent among those with obstructive sleep apnea (OSA) and are the leading cause of death in these individuals. However, due to clinical confounders, the mechanism by which OSA induces CVD is still unclear. Previous studies have shown that chronic intermittent hypoxia (CIH) and high cholesterol diet (HCD) induce distinct characteristics of atherosclerotic plaques, highlighting the specific mechanisms involved in CIH-induced vascular endothelial injury.

MATERIALS AND METHODS: This study aims to investigate whether nicotinamide adenine dinucleotide (NAD^+) biosynthesis reduction-mediated mitochondrial dysfunction is responsible for vascular endothelial injury induced by CIH and to elucidate its specific role in this process. Models were established to stimulate human umbilical vein endothelial cells (HUVECs) with CIH and oxidized low-density lipoprotein (ox-LDL), and the NAD^+ biosynthesis-related indicators, such as NAD^+ levels and nicotinamide phosphoribosyltransferase (NAMPT) enzyme activity, were measured in this model. Additionally, interventions were performed by supplementing NAD^+ levels with nicotinamide mononucleotide (NMN), inhibiting NAD^+ synthesis with FK866, and evaluating mitochondrial function, oxidative stress status, vascular constriction and dilation function, and endothelial adhesion function in these models. A comparative study was conducted to assess the effects of these interventions.

RESULTS: We found that under CIH conditions, NAMPT enzyme activity was inhibited, leading to a reduction in NAD^+ biosynthesis and a decrease in NAD^+/NADH ratio. At the same time, CIH caused mitochondrial dysfunction in HUVECs, including a decrease in adenosine triphosphate (ATP) content and mitochondrial membrane potential, as well as the activity of respiratory chain complex I and III, induced an increase in oxidative stress levels in endothelial cells, impaired vascular constriction and dilation function, and significantly increased expression of adhesion factors. The impact of CIH on endothelial cell-related mitochondrial function and endothelial function was restored by supplementing NMN. Although ox-LDL also causes multi-level endothelial injury, it does not involve the NAD^+ pathway, as there were no significant changes in the related indicators, and the impaired endothelial function under ox-LDL conditions was not restored by supplementing NMN.

CONCLUSIONS: CIH-induced vascular endothelial injury may be associated with NAD^+ biosynthesis reduction-mediated mitochondrial dysfunction. Supplementing NAD^+ precursors to increase its levels may be a potential intervention to ameliorate CIH-induced vascular endothelial injury, while it does not have a significant effect on endothelial injury caused by ox-LDL.

Key Words:
Obstructive sleep apnea, NAD^+, Mitochondrial dysfunction, Vascular endothelial injury.

Introduction

Cardiovascular complications due to obstructive sleep apnea (OSA) are of widespread concern. Chronic intermittent hypoxia (CIH) is the main pathological and physiological basis of OSA[1-4], and it is a key mediator in the development of cardiovascular diseases (CVD) associated with OSA[5]. Preliminary research[6] indicates that in mice with a deficiency of the ApoE gene, atherosclerosis induced by CIH, compared to atherosclerosis induced by a high cholesterol diet (HCD), differs significantly in terms of plaque morphology, cell composition and type of fibrous deposition. Impairment of vascular endothelial functions as an initiating factor for atherosclerosis formation

Corresponding Author: Dongmei Song, MD, Ph.D; e-mail: songdongmei@hebmu.edu.cn

due to OSA also varies between the two exposure groups, suggesting that atherosclerosis induced by CIH develops through a pathway that is distinct from atherosclerosis induced *via* an HCD. However, in clinical practice, CIH in the OSA population often coexists with multiple other cardiovascular risk factors[7], including smoking, obesity, and metabolic disorders, leading to increased CVD events[8]. The specific mechanism and relationship between solitary CIH and CVD are not yet clear. Therefore, it is particularly important to clarify the relationship between CIH and vascular endothelial injury and to determine the important role and potential mechanism that CIH plays in this process, in order to identify new targets for the prevention and treatment of this disease.

In the field of CIH research, the theory of oxidative stress has been one of the hotspots in recent years in studying the mechanisms related to vascular endothelial injury caused by CIH. The periodic changes of rapid hypoxia and reoxygenation in CIH are similar to local ischemia-reperfusion. During this process, a large amount of oxygen free radicals is produced, which disrupts the balance between the oxidative system and the antioxidant system, causing oxidative stress[9-11], leading to apoptosis of endothelial cells, increasing the susceptibility of the vascular wall to atherosclerosis, and ultimately leading to thrombosis formation[12]. Recently, it has been discovered[13] in the field of oxidative stress damage that nicotinamide phosphoribosyltransferase (NAMPT), which mediates nicotinamide adenine dinucleotide (NAD+) salvage pathways, plays an important role in maintaining NAD^+ levels and cellular vitality under oxidative stress conditions. This has become a widely studied hotspot in oxidative stress damage. The NAD^+ salvage pathway is the main pathway of NAD^+ biosynthesis in mammals, and NAD^+ is a key cofactor in cellular redox reactions, serving as the hydrogen receptor of the mitochondrial electron transport chain. When NAD^+ decreases, it triggers electron leakage, leading to mitochondrial oxidative stress[14,15]. Concurrently, NAD^+ is involved in mitochondrial redox reactions as a coenzyme; hence, NAD^+ depletion leads to mitochondrial dysfunction, thereby exacerbating mitochondrial oxidative stress[16,17]. There are also research reports[18] showing that prolonged hypoxia leads to irreversible loss of neuronal function, and immediate metabolic damage to the NAD^+ cycle upon reoxygenation, leading to excessive oxidation of NADH. Studies[19] in aged rats have shown that supplementation with nicotinamide ribonucleotide (NMN) reduces levels of mitochondrial reactive oxygen species (ROS) and oxidative stress, which in turn alleviates ischemia-reperfusion injury. Exogenous NAD^+ supplementation protects cardiac myoblasts from hypoxia/reoxygenation injury[20,21]. Therefore, we suggest that the reduction in NAD^+ is due to the impact on the NAD^+ salvage pathway, which leads to mitochondrial dysfunction, and that this reduction in NAD^+ may play a key role in the vascular endothelial injury induced by CIH.

In this study, we used CIH and classical oxidized low-density lipoprotein (ox-LDL) to induce human umbilical vein endothelial cells (HUVECs) to construct *in vitro* models of CIH and HCD-induced vascular endothelial injury. We compared and analyzed the differential expression of key indicators in NAD^+ and its biosynthetic pathway to explore the specific mechanisms that differentiate CIH-induced vascular endothelial injury from ox-LDL-induced.

Materials and Methods

Cell Culture

HUVECs were acquired from the Cell Bank of the Chinese Academy of Sciences (Shanghai, China). These cells were cultured in DMEM (Solarbio, Beijing, China) containing 10% phosphate-buffered saline (PBS) (Biological Industries, Israel), 100 U/mL penicillin and 100 mg/mL streptomycin, and 4.5 g/L D-glucose, and incubated in a 37°C, 95% humidity, and 5% CO_2 cell culture incubator (Thermo Fisher Scientific, Waltham, CA, USA). When these cells were fused, they were sub-cultured at a 1:3 ratio in 75 cm^2 cell culture flasks (NEST, Wuxi, China), and the culture medium was replaced every two days. All procedures were performed under sterile conditions in a Class II biological safety cabinet (Heal Force, Shanghai, China). Before use, all materials and disposable items were disinfected with 75% ethanol.

Establishment of the CIH Model

In reference to relevant literature[22], combined with the characteristics of intermittent hypoxia pathological physiology in OSA sleep mode, HUVECs cultured *in vitro* were exposed to intermittent hypoxia in a cell culture chamber (MAWORDE, Heilongjiang, China) to simulate the state of OSA patients. According to the measurement of the oxygen sensor for different durations of

hypoxia exposure and different reoxygenation times after hypoxia, the oxygen partial pressure in the culture medium was determined to establish a single cycle of low oxygen condition. Different cyclic hypoxia periods were used to determine the optimal CIH condition by measuring the cell viability and hypoxia-inducible factor-1alpha (HIF-1α) protein expression under different periods.

Establishment of the ox-LDL Model

Using different concentrations of ox-LDL to intervene in HUVECs for 24 hours, the optimal condition for ox-LDL intervention on HUVECs was determined by measuring cell viability and lactate dehydrogenase (LDH) release under different concentrations of ox-LDL intervention.

NMN Preprocessing

NMN was obtained from Sigma Aldrich, and the NMN stock solution was prepared in double-distilled water and stored at -20°C before dilution to the final concentration for experiments. The experimental groups were as follows: control group, CIH control group, ox-LDL group, CIH+NMN pretreatment group, and ox-LDL pretreatment group. The NMN pretreatment group was pretreated with 0.5 mM NMN for 24 hours before conducting further experiments as planned.

Cell Proliferation and Cytotoxicity Testing

The CCK-8 (Solarbio, Beijing, China) was utilized to examine the cell viability in accordance with the manufacturer's instructions. A total of 100 μl of 1×10^4 HUVECs were seeded into each well of the 96-well plate and exposed to either different time intervals of CIH or normoxia, or different concentrations of drugs. Following the incubation, 10 μl of cholecystokinin octapeptide (CCK-8) solution was added to each well at different time points, with the culture medium as a blank control. The cells were then cultured further at 37°C without light for 1-4 hours. Using a microplate reader (Biotek, VT, USA), the optical density (OD450) was measured at a wavelength of 450 nm. The experimental incubation time was chosen based on the corresponding incubation time with appropriate absorbance values. The cell viability was quantified in percentages, with the mean and standard deviation calculated from three independent variables.

Lactate Dehydrogenase (LDH) Activity Measurement

The LDH assay kit (Beyotime, Shanghai, China) was utilized for assessing LDH activity in cells. HUVECs were seeded at a density of 1×10^4 cells per well in a 96-well plate and then subjected to 150 mg/ml ox-LDL, a blank control, or left untreated for 24 hours. Following the manufacturer's instructions, LDH activity analysis was performed. The absorbance values were read at 495 nm using the EPOCH 2 microplate spectrophotometer (Biotek, VT, USA).

Measurement of Intracellular Reactive Oxygen Species (ROS)

The intracellular ROS were measured using the fluorescent probe DCFH-DA (ROS detection kit, Jiancheng, Nanjing, China). 2',7'-dichlorofluorescin (DCFH) reacts with ROS to form the fluorescent product DCF. HUVECs were incubated with DCFH-DA staining solution (10 μmol/L) at 37°C in darkness for 30 minutes. After incubation, the culture medium was discarded, and the residual DCFH-DA was completely washed off with PBS. The cells were perfused with 500 ml of PBS and the fluorescence intensity was detected by a fluorescence spectrophotometer (Biotek, VT, USA) at excitation and emission wavelengths of 495 nm and 515 nm, respectively, representing the level of intracellular ROS. Images of intracellular ROS were captured using a fluorescence microscope (Olympus, Toyko, Japan) with a magnification of 200 times. The experiment was repeated three times.

Measurement of Intracellular Malondialdehyde (MDA) and Superoxide Dismutase (SOD) Activity

The cellular level of lipid peroxidation was measured by using the thio-barbituric acid reaction (TBARS) to determine the level of formation of its by-product, MDA. The MDA content was measured using a colorimetric method with MDA equivalent standards, where an adduct is formed with TBA. Butylated hydroxytoluene (BHT) was added to each test sample to prevent further lipid oxidation during sample processing and TBA reaction. The spectrophotometry method detected MDA production at 533 nm and expressed as nmol/mg. SOD activity was determined using the Fluka analytical kit and measured using a Victor™X spectrophotometer at a wavelength of 440 nm. The reduction capacity of water-soluble tetrazolium 1 (WST-1) was measured to determine Cu/ZnSOD and mitochondrial MnSOD activity, where the hypoxanthine/xanthine oxidase system generated superoxide anions in the absence or presence of 4 mmol/L Potassium Cyanide

(KCN). One unit of SOD activity was defined as the amount of enzyme required to cause half-maximal inhibition of WST-1 reduction. All procedures were performed according to the instructions of the respective manufacturers (MAD and SOD assay kit, Jiancheng, Nanjing, China).

Determination of Nitric Oxide (NO) and Endothelial Nitric Oxide Synthase (eNOS) Concentrations

According to the manufacturer's manual, the cell sediment suspension was collected to determine the NO concentration by measuring the concentrations of total nitrate and nitrite (NO detection kit, Jiancheng, Nanjing, China). This method is based on the reduction of nitrate by nitrate reductase to convert it to nitrite for the determination of the total NO content. After the reaction, the nitrite produced by the Griess reaction was detected by colorimetric analysis at 550 nm using an enzyme-linked immunosorbent assay. The NO concentration of each sample was calculated using the formula based on the standard sample concentration and the corresponding optical density. As mentioned earlier, the activity of eNOS in the collected HUVECs was evaluated by converting L-arginine to NO (eNOS detection kit, Jiancheng, Nanjing, China).

Determination of Mitochondrial NAD+ and NAD+/NADH Ratio

The levels of NAD^+ and NADH in the mitochondria were assessed using a NAD^+/NADH assay kit (Beyotime, Shanghai, China) following the manufacturer's protocol. The total amount of NAD^+ in the mitochondria was extracted from the extraction buffer, and both the samples and NADH standard were treated with ethanol dehydrogenase to convert all NAD^+ to NADH. After incubating them in a MTT [3-(4,5-dimethylthiazol-2-yl)-2,5-diphenyltetrazolium bromide] detection buffer for an hour at room temperature, the conversion of MTT to formazan was monitored by recording the absorbance at 570 nm (A570). The change in A570 readings and the NADH standard curve were used to compute the total NAD^+. To measure NADH levels, the samples were heated to 60°C for 30 minutes, cooled on ice, and then treated with dehydrogenase to decompose all NAD^+ while preserving NADH. The NADH levels in the samples were then quantified as described earlier. The NAD^+ concentration was calculated by subtracting the NADH value from the total NAD^+, and the NAD^+/NADH ratio was determined by dividing NAD^+ by NADH.

Measurement of Intracellular ATP Concentration

HUVECs (1×10^6 cells) were homogenized in ice-cold phosphate-buffered saline (pH 7.4) using a DIAX 600 tissue homogenizer (Heidolph, Germany). The homogenate was centrifuged at 2,500 rpm for 10 minutes at 4°C. The supernatant was collected, and the protein concentration was measured using the bicinchoninic acid (BCA) assay. The level of ATP products in HUVECs was measured using an ATP detection kit (Jiancheng, Nanjing, China) according to the manufacturer's instructions. The ATP concentration in the samples was divided by the protein concentration to eliminate errors caused by differences in protein concentration in the samples.

Mitochondrial Membrane Potential Detection

Evaluation of mitochondrial membrane potential (MMP) was carried out as previously described[23]. According to the manufacturer's instructions, the JC-1 MMP Assay Kit (Beyotime, Shanghai, China) was used to detect changes in the instability of the mitochondrial membrane. In brief, 1×10^6 cells were washed twice with Dulbecco's Modified Eagle Medium (DMEM) without FBS and then incubated with 500 μL of JC-1 staining solution at 5% CO_2 and 37°C for 20 min. After that, the free probe was removed by JC-1 staining buffer. Cell photos were obtained using a fluorescence microscope. In normal cells with intact mitochondria, red fluorescent compounds were formed, while in damaged cells, JC-1 remained in a monomeric state and displayed green fluorescence. The excitation and emission wavelengths for each fluorescent dye were selected according to the manufacturer's instructions. The fluorescence intensity was quantitatively analyzed using ImageJ software (NIH, Bethesda, USA), and the MMP was evaluated as the ratio of red to green fluorescence intensity.

Measurement of the Activity of Respiratory Chain Complexes I and III in Mitochondria

As described above, mitochondria are first separated[24]. In simple terms, HUVECs are homogenized in isolation buffer (1 mM EGTA, 215 mM mannitol, 75 mM sucrose, 0.1% BSA, 20 mM Hepes, pH 7.2). After differential centrifugation, the obtained mitochondria are further homogenized. To determine the activity of respiratory chain complexes I and III, corresponding assay kits are used. The procedure for measuring

the activity of complex I involves incubating the reaction mixture containing ubiquinone and reduced nicotinamide adenine dinucleotide (NADH) at 30°C for 3 minutes before adding 100 µl of the sample. The production of NAD^+ is then monitored *via* the immediate measurement of absorbance at 340 nm (A340). Background absorption is corrected by measuring absorbance at 380 nm (A380) at two time points. To determine the total activity of complex I, the change rate of the corrected A340 value (A340-A380) and the NAD^+ standard curve are used. To measure the non-specific activity of complex I for each sample, a parallel reaction with a special complex I inhibitor is added to the reaction mixture. The specific activity of complex I for each sample is calculated by subtracting non-specific activity from total complex I activity.

To assess the activity of complex III, a reaction mixture comprising fumarate ubiquinone and cytochrome c is incubated in darkness at room temperature for 10 minutes, followed by the addition of 100 µl of the sample. Subsequently, the absorbance at 550 nm (A550) is promptly measured to track the decline rate of cytochrome c production after incorporating the sample and allowing it to incubate for 5 minutes. The activity of complex III is estimated according to alterations in A550 values and the reduction of the cytochrome c reference curve.

Enzyme-Linked Immunosorbent Assay (ELISA)

According to the manufacturer's instructions, these kits (Fankewei, Shanghai, China) targeting specific human cytokines [intercellular adhesion molecule-1 (ICAM-1), vascular cell adhesion molecule-1 (VCAM-1), and NAMPT] were used. In brief, 50 µL of supernatant or cell precipitate suspension from HUVECs culture medium was collected and then added successively to coated wells on a 96-well plate with blank, diluted standards, or samples. Next, the plate was incubated with HRP-conjugated antibody for 30 minutes at 37°C, with the reaction being terminated with a stop solution. The absorbance at 450 nm (A450) was recorded using a microplate reader (Bioteck, EPOCH, USA), and the concentration of the relevant protein was calculated based on the standard curve.

Protein Extraction and Western Blot

As previously mentioned, the Western blotting technique was used[25]. For nuclear and cytoplasmic proteins, a nuclear and cytoplasmic extraction reagent kit (Beyotime, Shanghai, China) containing 1% Triton X-100 (Solarbio, Beijing, China) was added to the cells to dissolve the membrane and maintain the integrity of the nuclear membrane. The supernatant was then incubated at 4°C for 20 minutes, followed by the addition of 500 µl nuclear isolation buffer. The homogenate was centrifuged at 600 x g (10 minutes, 4°C) to separate the cytoplasmic and granular nucleic acid fractions from the supernatant. The proteins were then extracted using Radio-Immunoprecipitation Assay (RIPA) lysis buffer (Beyotime, Shanghai, China). According to the manufacturer's instructions, total proteins were extracted from cells using RIPA lysis buffer containing 10% benzene sulfonate fluoride. The protein concentration was determined using a BCA protein concentration assay kit (Solarbio, Beijing, China). Each protein sample of approximately 30 µg was separated by Sodium dodecyl-sulfate polyacrylamide gel electrophoresis (SDS-PAGE) and transferred onto the polyvinylidene fluoride (PVDF) membrane. The membrane was blocked with 5% non-fat milk (dissolved in Tris Buffered Saline with Tween 20 (TBST) at room temperature for 2 hours, followed by incubation with primary antibody against alkaline phosphatase [HIF-1α (Abcam; cat: ab192256 number, 1:1000)] overnight at 4°C. The membrane was washed three times with TBS-TWEEN 20 (1% TWEEN) and incubated with a secondary antibody, either horseradish peroxidase (HRP)-labeled goat anti-rabbit IgG (H+L) (Beyotime, cat: A0208; 1:2000) or HRP-labeled goat anti-mouse IgG (H+L) (Beyotime, cat: A0216; 1:2000) at room temperature for 1 hour. The immunoblot was visualized using the Odyssey infrared imaging system (Li-Cor Biosciences, Nebraska, USA). The band intensity on the Western blot was analyzed using the ImageJ software (NIH, Bethesda, USA) .

Statistical Analysis

All data analyses were conducted using SPSS 22.0 (IBM Corp., Armonk, NY, USA) software. Measurement data were represented as mean ± SEM. For pairwise comparisons, Student's *t*-test was utilized, while for intergroup comparisons, one-way analysis of variance (ANOVA) was utilized. The count data were expressed as percentages and examined using chi-square tests. The criteria for significance were set at $p < 0.05$.

Results

Establishment of an In Vitro Model of CIH-Induced and ox-LDL-Induced Endothelial Injury in HUVECs

A partial pressure of oxygen of 45.8 ± 1.7 mm Hg was used in the HUVECs culture chamber to create atmospheric oxygen conditions (21% O_2). Hypoxic oxygen conditions of 1% O_2 were then created and maintained for 60 minutes. The partial pressure of oxygen in the medium was subsequently increased to 96.5 ± 3.8 mm Hg to reoxygenate the chamber to 21% O_2 for about 30 minutes (Figure 1A). Cell viability measured by CCK-8 was 87.87% after this first hypoxia-reoxygenation cycle and decreased gradually to 58.49% at the 8th cycle (Figure 1B). The model was validated by measuring the expression of HIF-1α under the control and CIH conditions. The nuclear protein content of HIF-1α was significantly higher ($p < 0.05$) in the CIH group after 8 cycles of intermittent hypoxia than in the normoxic group (Figure 1C-D). Therefore, 8 hypoxia-reoxygenation cycles were used for subsequent experiments.

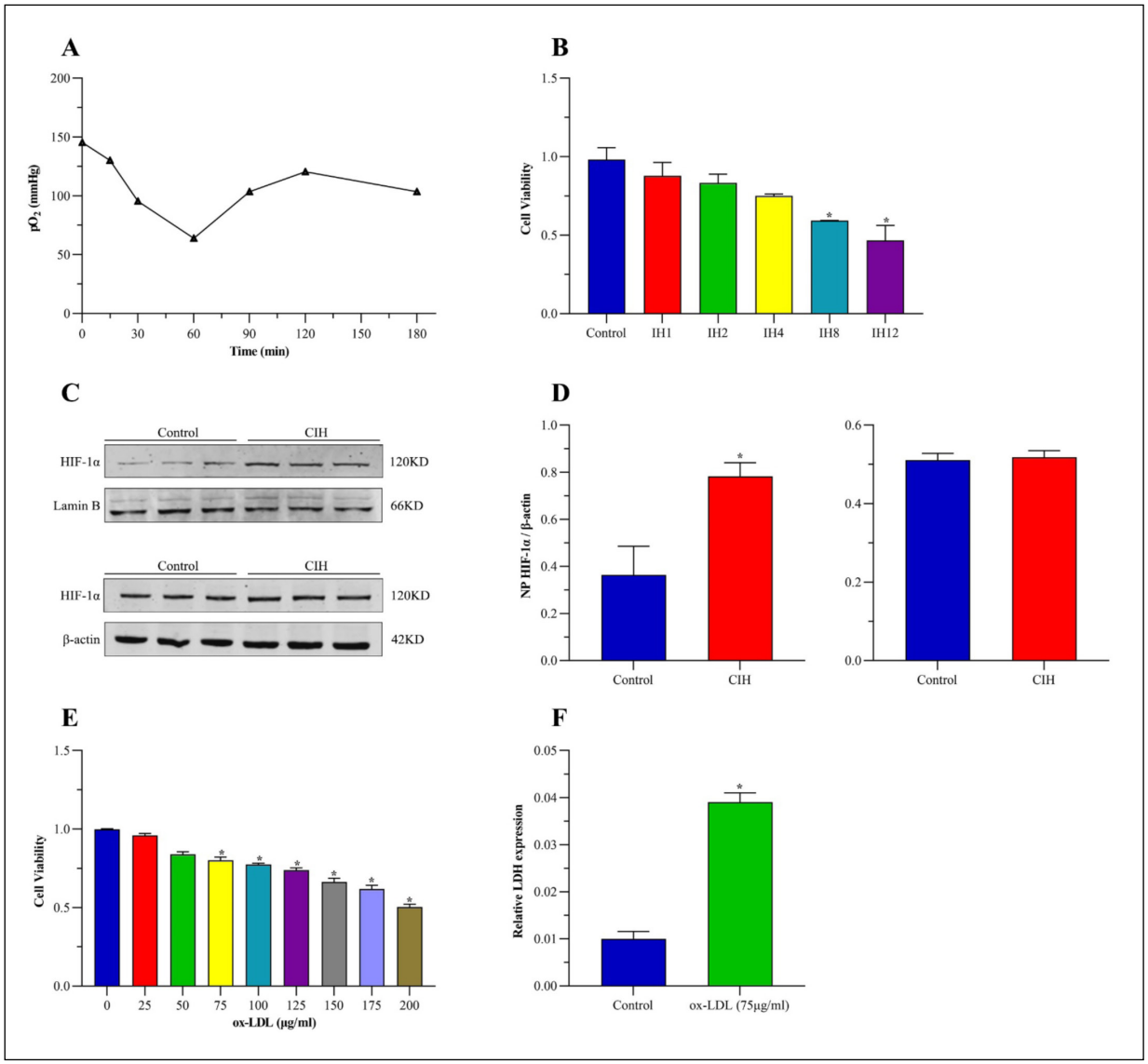

Figure 1. Establishment of *in vitro* model of endothelial injury induced by CIH and ox-LDL. **A**, Measurement of oxygen partial pressure in HUVECs culture media under different hypoxia and reoxygenation time points. **B**, Effects of different cycles of CIH intervention on cell viability in HUVECs. **C-D**, Detection of protein levels of HIF-1α in the cytoplasm and cell membrane under normal control group and 8 cycles of CIH condition using immunoblotting. **E**, Effects of different concentrations of ox-LDL on cell viability in HUVECs. **F**, Expression of LDH after ox-LDL treatment in HUVECs detected by ELISA. * *vs.* Control.

In a second model, ox-LDL was used to induce a classic model of endothelial cell injury in HUVECs. Ox-LDL treatment gradually decreased the cell viability of HUVECs in a concentration-dependent manner, with a significant decrease in cell viability at 75, 100, 125, and 150 μg/ml (Figure 1E). This model was validated using the release of lactate dehydrogenase (LDH) from cells as a marker of impaired cell function. The amount of LDH released from HUVECs at ox-LDL concentrations of 75 μg/ml was approximately 4 times higher than that of the control group (Figure 1 F). Therefore, 75 μg/ml of ox-LDL was used for subsequent experiments.

Effects on NAD+ and the NAD+ Salvage Synthetic Pathway Under CIH and ox-LDL Conditions

To verify whether NAD^+ levels and the NAD^+ salvage pathway are impaired in CIH-induced endothelial injury, we examined the expression levels of NAD^+ and its key enzyme in the salvage synthetic pathway, nicotinamide phosphoribosyltransferase (NAMPT), in HUVECs injury models induced by CIH and by ox-LDL. Intracellular NAD^+ levels were significantly reduced in the CIH group, the NAD^+/NADH ratio decreased, and the NAMPT activity decreased from 77.15 U/L to 57.31 U/L; the above indicators were statistically significantly different ($p < 0.05$) in the CIH group compared with the control group (Figure 2A-C). There was not, however, a statistically significant difference in any of these indices under the ox-LDL condition compared with the control group. Thus, CIH and ox-LDL exhibited different effects on NAD^+ and the NAD^+ salvage synthetic pathway, also indicating that CIH may inhibit the NAD^+ salvage pathway, leading to reduced NAD^+ levels and suggesting that the NAMPT-mediated NAD^+ salvage pathway may have an important role in CIH.

Effects on Mitochondrial Function Under CIH and ox-LDL Conditions, and After NMN Supplementation

To determine whether reduced NAD^+ levels affect mitochondrial function in endothelial cells under CIH and ox-LDL conditions, we examined mitochondrial function-related indices under CIH or ox-LDL stimulation. We also supplemented with NMN in HUVECs under CIH and ox-LDL conditions for further validation. First, the stimulated HUVECs were incubated with a fluorescent probe JC-1. Compared with the control group, the cells induced by the CIH and ox-LDL groups showed reduced red fluorescence and increased green fluorescence, and the ratio of red to green fluorescence was significantly decreased, indicating a decrease in MMP (Figure 3A,B). In addition, the ATP content was reduced by 43.24% in the CIH group compared with the control group (Figure 3C), accompanied by a decrease in the activity of mitochondrial respiratory chain complexes I and III. However, the ATP content and activity of mitochondrial respiratory chain complexes I and III in the ox-LDL group were not significantly different from the control group (Figure 3D-E). After NMN intervention, red fluorescence increased, and green fluorescence decreased in the CIH group indicating an increase in the level of MMP. The ATP content and mitochondrial respiratory chain complexes I and III activities increased after MNM intervention in this group. No significant changes in these indices were observed in the ox-LDL group after pretreatment with NMN (Figure 3A-E).

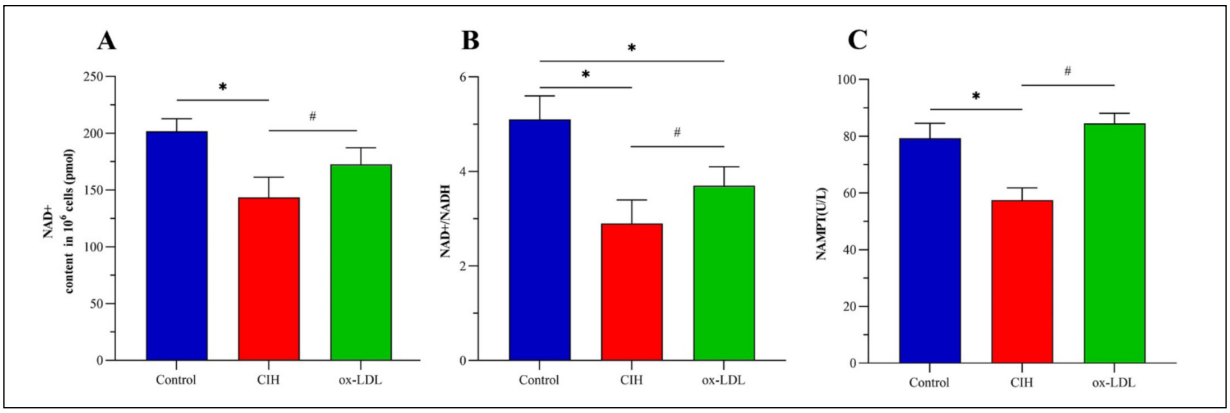

Figure 2. The effects of NAD^+ and its rescue pathways under CIH and ox-LDL conditions. A, Levels of NAD^+ in the culture supernatants of HUVECs under different conditions; (**B**) Ratios of NAD^+/NADH under different conditions; (**C**) Levels of NAMPT in the culture supernatants of HUVECs under different conditions. *vs. Control; #vs. CIH.

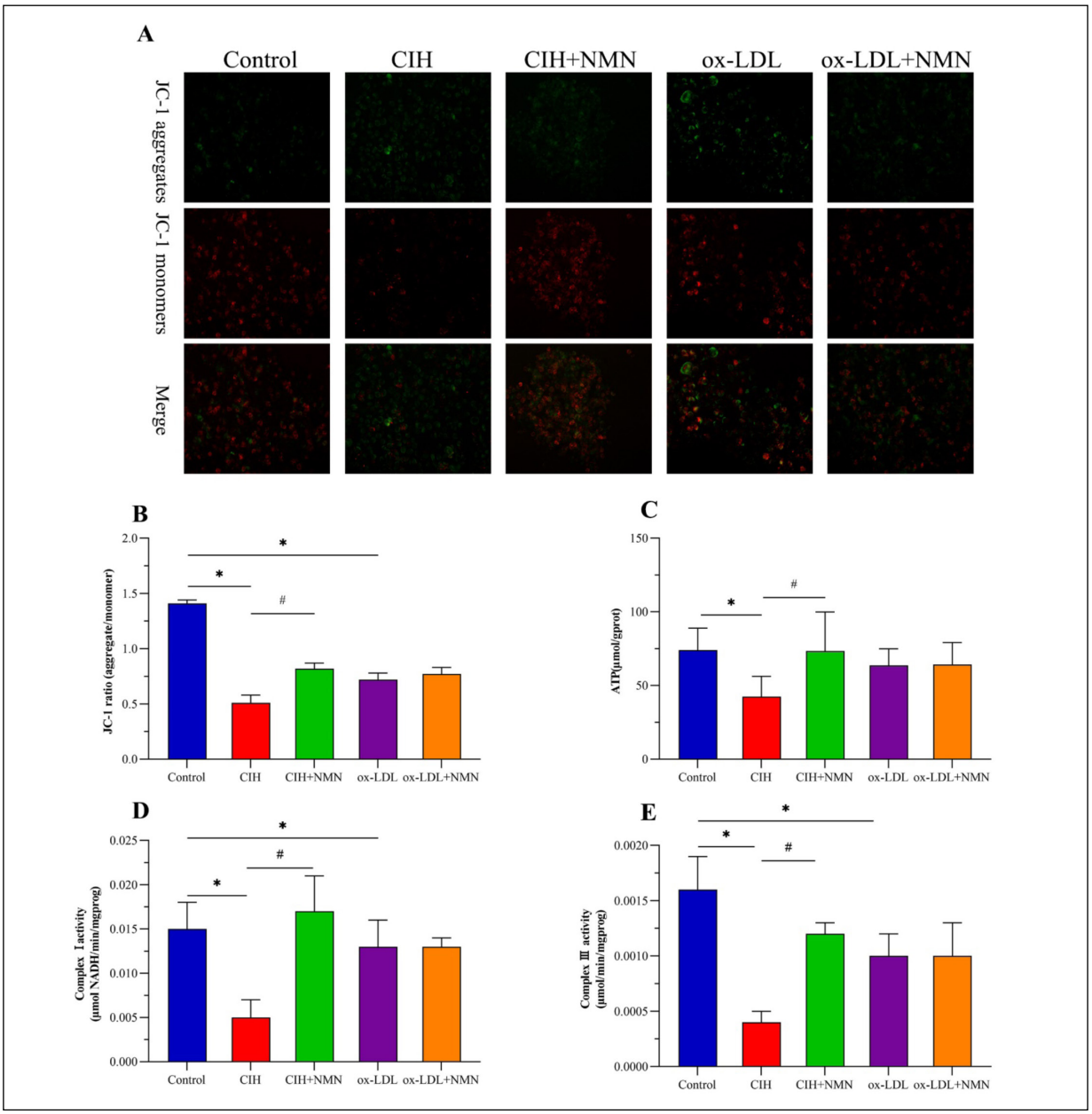

Figure 3. The differential effects of CIH and ox-LDL on mitochondrial function. **A-E**, After treatment with CIH and ox-LDL, HUVECs were supplemented with NMN under the same conditions. The effects of these conditions on mitochondrial membrane potential, activity of respiratory chain complexes I and III and ATP levels were measured. *vs. Control; #vs. CIH. MV: 40×.

Effects on Vascular Endothelial Function Under CIH and ox-LDL, and After NMN Supplementation

To assess the effect of NAD^+ levels on the state of oxidative stress of endothelial cells under CIH and ox-LDL conditions, we incubated stimulated HUVECs with the fluorescent probe DHR and measured ROS levels, MDA levels, and activity of the antioxidant enzyme SOD. In the CIH group, ROS levels increased by 52.23%, MDA levels increased from 1.16 nmol/ml to 1.48 nmol/ml, and SOD activity decreased by 29%, and these changes were significantly different compared to the control group ($p < 0.05$) (Figure 4A-D). In the ox-LDL group, ROS levels increased by 36.96%, MDA levels increased from 1.16 nmol/ml to 2.58 nmol/ml, and SOD activity decreased by 41.81%, and these changes were significantly different compared to the control group ($p < 0.05$) (Figure 4A-D). NMN

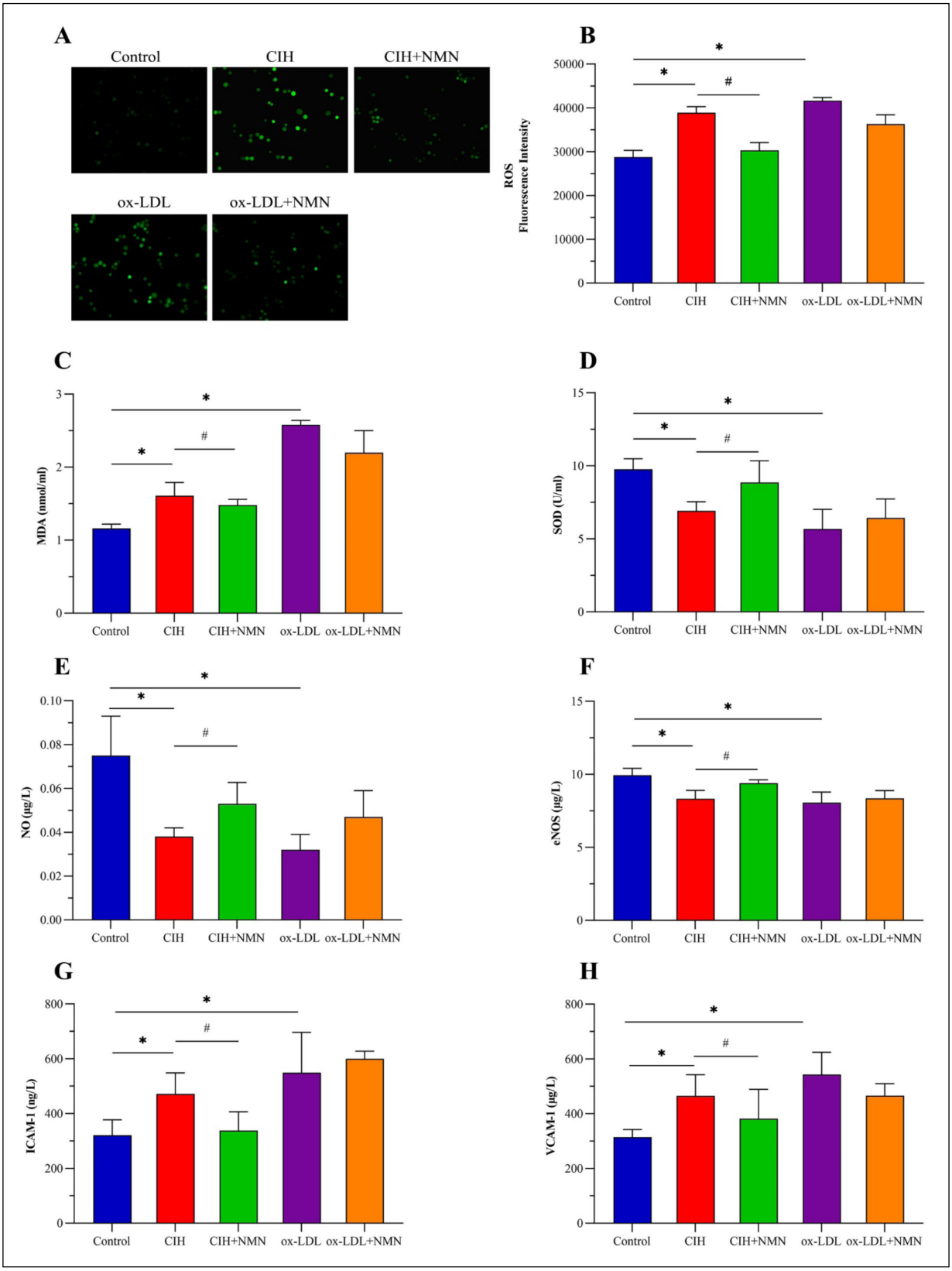

Figure 4. Under CIH and ox-LDL, as well as supplementation with NMN, differential effects on endothelial function were observed at various levels. **A-D**, The levels of ROS, MDA, and SOD activity within the cells. **E-F**, The levels of endothelial NO and eNOS content within the cells. **G-H**, The levels of ICAM-1 and VCAM-1. **vs.* Control; *#vs.* CIH. MV: 40×

intervention significantly suppressed the increase in ROS level, restored the activity of the antioxidant enzyme SOD, and inhibited the increase in MDA levels observed without MNM intervention in the CIH group. In the ox-LDL group, no significant changes in ROS, MDA content, and SOD activity were observed after NMN intervention. These findings suggest CIH may specifically cause oxidative stress injury in the vascular endothelium through the NAD^+ salvage pathway.

ELISA was used to measure levels of NO and eNOS in CIH- and ox-LDL-exposed conditions to assess whether endothelial diastolic function was altered. Levels of NO and eNOS decreased in the CIH group, by 28.30% and 26.19%, respectively, and in the ox-LDL group, by 28.93% and 39.61%, respectively, and these changes were significantly different compared to the control group ($p < 0.05$). However, after NMN intervention, eNOS and NO levels were restored in the CIH group but not in the ox-LDL group (Figure 4E-F).

To determine the effect of the above conditions on endothelial inflammatory adhesion molecules, we determined the levels of VCAM-1 and ICAM-1 using ELISA under the two experimental conditions compared to the control. As shown in Figure 4G-H, the expression of VCAM-1 and ICAM-1 was significantly higher under CIH and ox-LDL compared to the control groups ($p < 0.05$). However, while subsequent NMN intervention significantly reduced these two indices under CIH conditions, they were not significantly changed under ox-LDL conditions.

These findings suggest that CIH may induce impaired vascular endothelial diastolic and adhesive functions by specifically affecting the NAD^+ salvage pathway, whereas ox-LDL, a strong inducer of endothelial injury, may be mediated through other pathways.

Discussion

Clinical and basic studies in the literature surrounding the common risk factors, pathological evolution, and underlying mechanisms of OSA have demonstrated that vascular endothelial injury induced by CIH plays an important role in OSA-related CVD. However, these studies have been unable to determine the underlying mechanisms of how CIH induces endothelial injury, as CIH is confounded with other risk factors, obscuring the specific role of CIH on vascular injury. Therefore, it was important to investigate the mechanism of action of CIH-induced vascular endothelial injury. In the present study, we compared CIH to its classic inducing factor ox-LDL as a control to explore and highlight the specificity of the CIH mechanism in this process. Our results showed that the NAMPT-mediated NAD^+ salvage pathway was impaired in CIH-induced HUVECs, which in turn led to NAD^+ reduction. However, the addition of NMN effectively reversed the multifaceted endothelial functional impairment under CIH conditions but did not significantly affect ox-LDL-induced conditions. These results suggest that CIH and ox-LDL may mediate vascular injury through different mechanisms, with CIH potentially inhibiting the NAD^+ salvage pathway, leading to a decrease in NAD^+ levels, which in turn leads to endothelium-related functional impairment through the induction of mitochondrial dysfunction.

OSA, characterized by rapid reoxygenation after hypoxia, is the main mechanism leading to the generation of oxidative stress and is the mechanism most intensively studied in CIH-mediated vascular injury[26,27]. Mitochondria are one of the major organelles of cellular energy metabolism. Although endothelial cells do not derive most of their energy from mitochondrial oxidative phosphorylation metabolism, mitochondria in endothelial cells are still physiologically relevant, in part because they are the major source of cellular ROS, in addition to the NOX system. NAD^+ is essential for the electron transport reaction in mitochondria, which produce ATP through the Krebs cycle, fatty acid oxidation, and oxidative phosphorylation. NAD^+ deficiency inhibits mitochondrial function and ATP production, as well as facilitating increased mtROS production, which in turn can accelerate inflammation and lead to impairment of vascular endothelial functions[28,29]. Recent studies[14,30] have shown that the NAD^+ salvage pathway is affected and subsequently mediated by oxidative stress and promotes the development of endothelial injury in hypoxic environments. Similarly, a decrease in NAD^+ levels can induce mitochondrial oxidative stress, leading to endothelial injury in mouse arteries[31,32]. NAD^+ level downregulation resulting in mitochondrial oxidative stress may induce the decrease of vascular endothelial function and the appearance of related phenotypes. The production of higher concentrations of ROS after impaired mitochondrial function can lead to and exacerbate oxidative stress and secondary cellular damage[33-35]. For example, oxygen radicals react with biofilms *via* lipid peroxidation of un-

saturated fats to generate MDA, which causes a decrease in SOD, the main antioxidant enzyme against reactive oxygen metabolites, further participating in the formation of atherosclerosis[36]. Similarly, in our study, we showed that CIH leads to mitochondrial dysfunction in HUVECs, as evidenced by a significant decrease in mitochondrial complexes I and III, ATP content, and MMP levels. These findings strongly support the inhibition of the NAD^+ salvage pathway, leading to a reduction in NAD^+, as playing a direct role in vascular endothelial mitochondrial dysfunction caused by CIH, and that this mechanism is different from that observed under the classic ox-LDL condition. Certain pathways may be able to maintain mitochondrial NAD^+ levels and thus play a role in maintaining mitochondrial function under the classic condition.

The inhibition of the NAMPT-mediated NAD^+ biosynthesis pathway can downregulate antioxidant proteins, leading to increased oxidative stress sensitivity[37,38]. Oxidative stress leads to cytokine secretion and promotes inflammation in vascular tissues, while the upregulation of adhesion molecules such as ICAM-1 and VCAM-1 stimulates endothelial activation by promoting leukocyte adhesion to endothelial cells[39,40]. In the present study, we also found a significant increase in ROS and MDA in HUVECs under CIH and ox-LDL conditions, while SOD enzyme activity was significantly downregulated, accompanied by a significant increase in both ICAM-1 and VCAM-1 expression. We speculate that decreased NAD^+ levels may generate higher ROS by inducing a decrease in mitochondrial function, as well as leading to a decrease in cellular antioxidant capacity, ultimately causing an increase in oxidative stress and levels of inflammatory factors in HUVECs under CIH conditions, leading to impaired endothelial function. Vascular endothelial injury is characterized by reduced bioavailability of endothelium-derived vasoactive mediators and NO[41]. The expression of eNOS, a synthase of NO, has also been used as an important index to evaluate endothelial function[42]. The present study also observed a significant reduction in NO and eNOS under CIH conditions, and these findings suggest that the CIH-induced NAMPT-mediated NAD^+ salvage pathway caused by CIH is likely to be responsible for its contribution to vascular endothelial injury. Research[43] has demonstrated that specific inhibition of NAD^+-dependent sirtuin 1 (SIRT1) in mouse arterial endothelium leads to a decrease in NO and inhibition of endothelium-dependent vasodilation and *in vitro* experiments[44] have revealed that SIRT1 can increase endothelial NO through direct deacetylation. These processes stimulate the activity of endothelial NO synthase and exert a direct protective effect on endothelium-dependent vascular activity, a process that, in addition to the role of NAD^+ in the maintenance of mitochondrial dysfunction, may provide indirect evidence that reduced NAD^+ levels may lead to the impairment of endothelial functions through another mechanism affecting SIRT1.

Evidence[45-48] is accumulating, demonstrating that increasing NAD^+ levels through supplementation with NAD^+ intermediates can improve cardiovascular-related endothelial injury. In addition, studies[49,50] have found that treatment of aged mice with NMN restored endothelium-dependent diastolic function in the carotid artery. To identify the NAMPT-mediated decrease in NAD^+ levels as the cause of impaired endothelial function due to CIH, we performed back-supplementation of HUVECs under CIH and ox-LDL conditions with NMN. Results verified that back-supplementation of NAD^+ reversed CIH-induced mitochondrial dysfunction, oxidative stress, and endothelial injury in endothelial cells.

Limitations

There are some limitations to this study. First, we were only able to demonstrate a correlation between NAD^+ levels that were reduced under CIH conditions and concomitant vascular endothelial injury. Whether other causes are involved, and the specific mechanisms involved remain to be explored. Second, in addition to the NAD^+ salvage pathway, the effects of other synthetic pathways, including the de novo synthesis of NAD^+ and NAD^+-consuming enzymes on NAD^+ levels, were not assessed. In addition, the downstream mechanisms of vascular endothelial injury due to the NAD^+ salvage pathway require further investigation.

Conclusions

Our study has shown that CIH-induced vascular endothelial injury may be associated with a decrease in NAMPT-mediated NAD^+ levels, leading to mitochondrial dysfunction, followed by increased oxidative stress and increased vascular adhesion, and that supplementation of NAD+ precursors to increase their levels may be a potential intervention to ameliorate CIH-induced vascular endothelial injury.

Conflict of Interest
None.

Ethics Approval
The study was conducted in accordance with the Declaration of Helsinki, and approved by the Internal Review Board of The First Hospital of Hebei Medical University (Ethics approval No.: 20200623).

Informed Consent
Not applicable.

Funding
This research was funded by Hebei Province Natural Science Foundation of China (Grant number H2023206407), S&T Program of Hebei (Grant number 21377734D) and Training Programme Foundation for the Talents of clinical medicine sponsored by the Government (Grant number ZF2024128).

Authors' Contributions
All authors contributed to study conception and design. Experiment were performed by Zhitao Fan, Yinghao Niu, Weiwei Chi and Guangli Wu. The first draft of the manuscript was written by Zhitao Fan. Liping Dong and Dongmei Song reviewed and edited previous versions of the manuscript. All authors read and approved the final version of the manuscript.

Data Availability
The datasets generated during and/or analyzed during the current study are available from the corresponding author on reasonable request.

ORCID ID
Zhitao Fan: 0000-0002-8258-1069
Liping Dong: 0000-0002-0907-7464
Yinghao Niu: 0009-0004-3823-1063
Weiwei Chi: 0009-0003-2424-7331
Guangli Wu: 0000-0001-7172-5605
Dongmei Song: 0000-0002-2183-1730.

References

1) Drager LF, Polotsky VY, Lorenzi-Filho G. Obstructive sleep apnea: an emerging risk factor for atherosclerosis. Chest 2011; 140: 534-542.
2) McNicholas WT, Bonsigore MR; Management Committee of EU COST ACTION B26. Sleep apnoea as an independent risk factor for cardiovascular disease: current evidence, basic mechanisms and research priorities. Eur Respir J 2007; 29: 156-178.
3) Ralls F, Cutchen L. A contemporary review of obstructive sleep apnea. Curr Opin Pulm Med 2019; 25: 578-593.
4) Bradley TD, Floras JS. Obstructive sleep apnoea and its cardiovascular consequences. Lancet 2009; 373: 82-93.
5) Lebkuchen A, Freitas LS, Cardozo KHM, Drager LF. Advances and challenges in pursuing biomarkers for obstructive sleep apnea: Implications for the cardiovascular risk. Trends Cardiovasc Med 2021; 31: 242-249.
6) Song D, Fang G, Greenberg H, Liu SF. Chronic intermittent hypoxia exposure-induced atherosclerosis: a brief review. Immunol Res 2015; 63: 121-130.
7) Barros D, García-Río F. Obstructive sleep apnea and dyslipidemia: from animal models to clinical evidence. Sleep 2019; 42: zsy236.
8) Savransky V, Nanayakkara A, Li J, Bevans S, Smith PL, Rodriguez A, Polotsky VY. Chronic intermittent hypoxia induces atherosclerosis. Am J Respir Crit Care Med 2007; 175: 1290-1297.
9) Siti HN, Kamisah Y, Kamsiah J. The role of oxidative stress, antioxidants and vascular inflammation in cardiovascular disease (a review). Vascul Pharmacol 2015; 71: 40-56.
10) Lavie L, Lavie P. Molecular mechanisms of cardiovascular disease in OSAHS: the oxidative stress link. Eur Respir J 2009; 33: 1467-1484.
11) Lavie L. Oxidative stress in obstructive sleep apnea and intermittent hypoxia--revisited--the bad ugly and good: implications to the heart and brain. Sleep Med Rev 2015; 20: 27-45.
12) Luo B, Li Y, Zhu M, Cui J, Liu Y, Liu Y. Intermittent Hypoxia and Atherosclerosis: From Molecular Mechanisms to the Therapeutic Treatment. Oxid Med Cell Longev 2022; 3: 1438470.
13) Dölle C, Skoge RH, Vanlinden MR, Ziegler M. NAD biosynthesis in humans--enzymes, metabolites and therapeutic aspects. Curr Top Med Chem 2013; 13: 2907-2917.
14) Burgos ES. NAMPT in regulated NAD biosynthesis and its pivotal role in human metabolism. Curr Med Chem 2011; 18: 1947-1961.
15) Garten A, Schuster S, Penke M, Gorski T, de Giorgis T, Kiess W. Physiological and pathophysiological roles of NAMPT and NAD metabolism. Nat Rev Endocrinol 2015; 11: 535-546.
16) Dröse S, Brandt U. Molecular mechanisms of superoxide production by the mitochondrial respiratory chain. Adv Exp Med Biol 2012; 748: 145-169.
17) Cogliati S, Frezza C, Soriano ME, Varanita T, Quintana-Cabrera R, Corrado M, Cipolat S, Costa V, Casarin A, Gomes LC, Perales-Clemente E, Salviati L, Fernandez-Silva P, Enriquez JA, Scorrano L. Mitochondrial cristae shape determines respiratory chain supercomplexes assembly and respiratory efficiency. Cell 2013; 155: 160-171.
18) Pérez-Pinzón MA, Mumford PL, Sick TJ. Prolonged anoxic depolarization exacerbates NADH hyperoxidation and promotes poor electrical recovery after anoxia in hippocampal slices. Brain Res 1998; 786: 165-170.

19) Khaidizar FD, Nakahata Y, Kume A, Sumizawa K, Kohno K, Matsui T, Bessho Y. Nicotinamide phosphoribosyltransferase delays cellular senescence by upregulating SIRT1 activity and antioxidant gene expression in mouse cells. Genes Cells 2017; 22: 982-992.

20) Liu L, Wang P, Liu X, He D, Liang C, Yu Y. Exogenous NAD(+) supplementation protects H9c2 cardiac myoblasts against hypoxia/reoxygenation injury via Sirt1-p53 pathway. Fundam Clin Pharmacol 2014; 28: 180-189.

21) Lai YF, Wang L, Liu WY. Nicotinamide pretreatment alleviates mitochondrial stress and protects hypoxic myocardial cells via AMPK pathway. Eur Rev Med Pharmacol Sci 2019; 23: 1797-1806.

22) Martinez CA, Kerr B, Jin C, Cistulli PA, Cook KM. Obstructive Sleep Apnea Activates HIF-1 in a Hypoxia Dose-Dependent Manner in HCT116 Colorectal Carcinoma Cells. Int J Mol Sci 2019; 20: 445.

23) Zhou P, Xie W, Luo Y, Lu S, Dai Z, Wang R, Sun G, Sun X. Protective Effects of Total Saponins of Aralia elata (Miq.) on Endothelial Cell Injury Induced by TNF-α via Modulation of the PI3K/Akt and NF-κB Signalling Pathways. Int J Mol Sci 2018; 20: 36.

24) Zhang X, Dash RK, Jacobs ER, Camara AKS, Clough AV, Audi SH. Integrated computational model of the bioenergetics of isolated lung mitochondria. PLoS One 2018; 13: e0197921.

25) Xie W, Meng X, Zhai Y, Ye T, Zhou P, Nan F, Sun G, Sun X. Antidepressant-like effects of the Guanxin Danshen formula via mediation of the CaMK II-CREB-BDNF signalling pathway in chronic unpredictable mild stress-induced depressive rats. Ann Transl Med 2019; 7: 564.

26) Meliante PG, Zoccali F, Cascone F, Di Stefano V, Greco A, de Vincentiis M, Petrella C, Fiore M, Minni A, Barbato C. Molecular Pathology, Oxidative Stress, and Biomarkers in Obstructive Sleep Apnea. Int J Mol Sci 2023; 24: 5478.

27) Orrù G, Storari M, Scano A, Piras V, Taibi R, Viscuso D. Obstructive Sleep Apnea, oxidative stress, inflammation and endothelial dysfunction-An overview of predictive laboratory biomarkers. Eur Rev Med Pharmacol Sci 2020; 24: 6939-6948.

28) Csiszar A, Tarantini S, Yabluchanskiy A, Balasubramanian P, Kiss T, Farkas E, Baur JA, Ungvari Z. Role of endothelial NAD+ deficiency in age-related vascular dysfunction. Am J Physiol Heart Circ Physiol 2019; 316: H1253-H1266.

29) Tannous C, Booz GW, Altara R, Muhieddine DH, Mericskay M, Refaat MM, Zouein FA. Nicotinamide adenine dinucleotide: Biosynthesis, consumption and therapeutic role in cardiac diseases. Acta Physiol (Oxf) 2021; 231: e13551.

30) Abdellatif M, Trummer-Herbst V, Koser F, Durand S, Adão R, Vasques-Nóvoa F, Freundt JK, Voglhuber J, Pricolo MR, Kasa M, Türk C, Aprahamian F, Herrero-Galán E, Hofer SJ, Pendl T, Rech L, Kargl J, Anto-Michel N, Ljubojevic-Holzer S, Schipke J, Brandenberger C, Auer M, Schreiber R, Koyani CN, Heinemann A, Zirlik A, Schmidt A, von Lewinski D, Scherr D, Rainer PP, von Maltzahn J, Mühlfeld C, Krüger M, Frank S, Madeo F, Eisenberg T, Prokesch A, Leite-Moreira AF, Lourenço AP, Alegre-Cebollada J, Kiechl S, Linke WA, Kroemer G, Sedej S. Nicotinamide for the treatment of heart failure with preserved ejection fraction. Sci Transl Med 2021; 13: eabd7064.

31) Li Y, Li J, Zhao C, Yang L, Qi X, Wang X, Zhou Q, Shi W. Hyperglycemia-reduced NAD+ biosynthesis impairs corneal epithelial wound healing in diabetic mice. Metabolism 2021; 114: 154402.

32) Diguet N, Trammell SAJ, Tannous C, Deloux R, Piquereau J, Mougenot N, Gouge A, Gressette M, Manoury B, Blanc J, Breton M, Decaux JF, Lavery GG, Baczkó I, Zoll J, Garnier A, Li Z, Brenner C, Mericskay M. Nicotinamide Riboside Preserves Cardiac Function in a Mouse Model of Dilated Cardiomyopathy. Circulation 2018; 137: 2256-2273.

33) Imai S. Nicotinamide phosphoribosyltransferase (Nampt): a link between NAD biology, metabolism, and diseases. Curr Pharm Des 2009; 15: 20-28.

34) Münzel T, Camici GG, Maack C, Bonetti NR, Fuster V, Kovacic JC. Impact of Oxidative Stress on the Heart and Vasculature: Part 2 of a 3-Part Series. J Am Coll Cardiol 2017; 70: 212-229.

35) Li H, Horke S, Förstermann U. Vascular oxidative stress, nitric oxide and atherosclerosis. Atherosclerosis 2014; 237: 208-219.

36) Huynh K, Bernardo BC, McMullen JR, Ritchie RH. Diabetic cardiomyopathy: mechanisms and new treatment strategies targeting antioxidant signaling pathways. Pharmacol Ther 2014; 142: 375-415.

37) Xu R, Yuan Z, Yang L, Li L, Li D, Lv C. Inhibition of NAMPT decreases cell growth and enhances susceptibility to oxidative stress. Oncol Rep 2017; 38: 1767-1773.

38) Feng J, Yan PF, Zhao HY, Zhang FC, Zhao WH, Feng M. Inhibitor of Nicotinamide Phosphoribosyltransferase Sensitizes Glioblastoma Cells to Temozolomide via Activating ROS/JNK Signaling Pathway. Biomed Res Int 2016; 2016: 1450843.

39) Costanzo A, Moretti F, Burgio VL, Bravi C, Guido F, Levrero M, Puri PL. Endothelial activation by angiotensin II through NFkappaB and p38 pathways: Involvement of NFkappaB-inducible kinase (NIK), free oxygen radicals, and selective inhibition by aspirin. J Cell Physiol 2003; 195: 402-410.

40) Maniaci A, Iannella G, Cocuzza S, Vicini C, Magliulo G, Ferlito S, Cammaroto G, Meccariello G, De Vito A, Nicolai A, Pace A, Artico M, Taurone S. Oxidative Stress and Inflammation Biomarker Expression in Obstructive Sleep Apnea Patients. J Clin Med 2021; 10: 277.

41) Félétou M, Vanhoutte PM. Endothelial dysfunction: a multifaceted disorder (The Wiggers Award Lecture). Am J Physiol Heart Circ Physiol 2006; 291: H985-H1002.

42) Förstermann U, Münzel T. Endothelial nitric oxide synthase in vascular disease: from marvel to menace. Circulation 2006; 113: 1708-1714.

43) Sebastián C, Satterstrom FK, Haigis MC, Mostoslavsky R. From sirtuin biology to human diseases: an update. J Biol Chem 2012; 287: 42444-42452.

44) Mattagajasingh I, Kim CS, Naqvi A, Yamamori T, Hoffman TA, Jung SB, DeRicco J, Kasuno K, Irani K. SIRT1 promotes endothelium-dependent vascular relaxation by activating endothelial nitric oxide synthase. Proc Natl Acad Sci U S A 2007; 104: 14855-14860.

45) Mateuszuk Ł, Campagna R, Kutryb-Zając B, Kuś K, Słominska EM, Smolenski RT, Chlopicki S. Reversal of endothelial dysfunction by nicotinamide mononucleotide via extracellular conversion to nicotinamide riboside. Biochem Pharmacol 2020; 178: 114019.

46) Yoshino J, Baur JA, Imai SI. NAD+ Intermediates: The Biology and Therapeutic Potential of NMN and NR. Cell Metab 2018; 27: 513-528.

47) Huang RX, Tao J. Nicotinamide mononucleotide attenuates glucocorticoid induced osteogenic inhibition by regulating the SIRT1/PGC 1α signaling pathway. Mol Med Rep 2020; 22: 145-154.

48) Hong W, Mo F, Zhang Z, Huang M, Wei X. Nicotinamide Mononucleotide: A Promising Molecule for Therapy of Diverse Diseases by Targeting NAD+ Metabolism. Front Cell Dev Biol 2020; 8: 246.

49) Yoshino J, Mills KF, Yoon MJ, Imai S. Nicotinamide mononucleotide, a key NAD(+) intermediate, treats the pathophysiology of diet- and age-induced diabetes in mice. Cell Metab 2011; 14: 528-536.

50) Rajman L, Chwalek K, Sinclair DA. Therapeutic Potential of NAD-Boosting Molecules: The In Vivo Evidence. Cell Metab 2018; 27: 529-547.